JOURNAL OF GEOPHYSICAL RESEARCH, VOL. 102, NO. D9, PAGES 10,637–10,651, MAY 20, 1997

Ozone production and transports in the tropical Atlantic region during the biomass burning season

Geert-Jan Roelofs and Jos Lelieveld
Institute for Marine and Atmospheric Research Utrecht, Utrecht, The Netherlands

Herman G. J. Smit and Dieter Kley
Institute for Chemistry of the Polluted Atmosphere, Jülich, Germany

Abstract. Tropospheric O_3 distributions over the Atlantic Ocean have been calculated with a coupled chemistry-general circulation model. Photochemically produced O_3, mainly from biomass burning emissions, dominates O_3 abundances over the tropical Atlantic Ocean in the southern hemisphere (SH) during September/October. On the other hand, O_3 of stratospheric origin strongly contributes to the tropospheric O_3 column at latitudes poleward of 30°S. Simulated tropospheric flow patterns are in good agreement with European Centre for Medium-Range Weather Forecasts analyses and trajectory studies. Tracer transports over the tropical South Atlantic Ocean are strongly influenced by wind shear between the boundary layer and the free troposphere, leading to a stratification of O_3. At the surface relatively O_3-poor air is transported from SH middle latitudes. At higher altitudes, relatively O_3-rich air is transported from the African biomass burning regions between 2 and 5 km and from South American biomass burning regions in the mid-to-upper troposphere. The model simulates O_3 production rates of 10–50 parts per billion by volume (ppbv) O_3 d^{-1} in the lower troposphere over the biomass burning regions and 2–6 ppbv O_3 d^{-1} in the middle and upper troposphere. Photochemical destruction of O_3 prevails in the lower troposphere over the ocean, maximizing in the African and South American outflow regions. In the northern hemisphere, in situ photochemically produced O_3 dominates throughout most of the troposphere. Calculated O_3 volume mixing ratios are compared with a latitude-altitude O_3 distribution measured during an Atlantic ship cruise along 30°W, between 55°N and 30°S, in September/October 1988, and with ozone sonde measurements from Southern African Fire Atmospheric Research Initiative/Transport and Atmospheric Chemistry Near the Equator—Atlantic (SAFARI/TRACE A) in September/October 1992. Calculated O_3 levels agree reasonably well with the ship cruise data, except for the tropical SH lower troposphere where the model significantly underestimates O_3. However, modeled vertical O_3 distributions are underpredicted compared to TRACE A sonde measurements. Simulated O_3 columns over the ocean are somewhat lower compared to values retrieved from satellite data, in particular over the tropical Atlantic. The underestimation is probably due to the neglect of higher hydrocarbon chemistry in the model.

1. Introduction

Relatively high O_3 levels over the southern hemisphere (SH) Atlantic Ocean in austral spring are related to biomass burning activities in South America and Africa, which maximize in the dry season [*Crutzen and Andreae*, 1990]. Tropospheric O_3 columns retrieved from satellite data are up to 50 Dobson units (DU) [*Fishman et al.*, 1990; *Hudson et al.*, 1995; *Kim et al.*, 1996]. Several studies have analyzed atmospheric transports over the SH tropical Atlantic Ocean and their influence on observed O_3 distributions. On the basis of a European Centre for Medium-Range Weather Forecasts (ECMWF) meteorological analysis, *Krishnamurti et al.* [1993] suggested that high O_3 abundances over the eastern Atlantic Ocean result from transports of biomass burning products from South America by high-altitude westerly winds as well as transports from Africa by lower-altitude easterly winds, followed by accumulation of O_3 under the influence of an anticyclone near the west coast of central Africa. On the basis of data from the measurement campaign Southern African Fire Atmospheric Research Initiative/Transport and Atmospheric Chemistry Near the Equator—Atlantic (SAFARI/TRACE A), conducted in September and October 1992, it was demonstrated that biomass burning in South America and Africa is the dominant source of O_3 precursors that lead to high O_3 abundances over the tropical South Atlantic Ocean. *Thompson et al.* [1996a] suggested that significant additional photochemical O_3 formation, 1–2 DU d^{-1}, takes place during transport over the ocean, resulting in larger O_3 columns over the ocean than over land. On the basis of a passive tracer simulation, *Krishnamurti et al.* [1993] proposed that transports of O_3 from stratospheric origin may also contribute significantly to tropospheric O_3 levels at middle latitudes.

Although several measurement series of surface O_3 and vertical profiles are available for background and polluted con-

Copyright 1997 by the American Geophysical Union.

Paper number 97JD00400.
0148-0227/97/97JD-00400$09.00

tinental conditions, especially in the northern hemisphere (NH) [*Komhyr et al.*, 1989; *Oltmans and Levy*, 1994] (World Ozone Data Center [see, e.g., *Logan*, 1994]), measurements of tropospheric O_3 over the remote oceans for longer periods of time are rather scarce. *Winkler* [1988] compiled a climatology of surface O_3 mixing ratios over the Atlantic Ocean from measurements carried out between 1977 and 1986 on board several research vessels. The total ozone mapping spectrometer (TOMS) minus stratospheric aerosol and gas experiment (SAGE) satellite retrieval of tropospheric O_3 columns by *Fishman et al.* [1990] provides valuable information on the horizontal distribution of tropospheric O_3. However, these data are subject to considerable uncertainty, especially for the extratropics. Further, *Hudson et al.* [1995] showed that thus retrieved tropospheric O_3 columns are overestimated when stratocumulus clouds are present and underestimated under cloud-free conditions when the lower troposphere contains large amounts of O_3. Both situations are common in the considered area.

Incidental measurement campaigns investigated O_3 distributions or concentrations for a limited period. Detailed vertical distributions of tropospheric O_3 were measured on board the German research vessel *Polarstern*. Ozone soundings were launched during ship cruises along the 30°W meridian between approximately 55°N and 30°S in March/April 1987 and September/October 1988 [*Smit et al.*, 1989, 1990]. Similar cruises have been carried out closer to the Atlantic coasts [*Weller et al.*, 1996]. Because instantaneous distributions were measured, details were strongly influenced by synoptic meteorological features, and their representativeness of monthly or seasonal distributions may be limited. Recently, a special issue of *Journal of Geophysical Research*, *101*(D19), 1996, appeared on the SAFARI/TRACE A measurement campaign conducted in September/October 1992. The goal of the SAFARI campaign, conducted in southern Africa, was a comprehensive study of trace gas and aerosol emissions from vegetation fires and the role of fires in atmospheric chemistry, climate, and ecology [*Lindesay et al.*, 1996]. During TRACE A the chemical composition, transport, and chemistry of the atmosphere over the tropical South Atlantic Ocean and the adjacent South American and African continents were studied [*Fishman et al.*, 1996a]. TRACE A measurements included vertical O_3 profiles from ozone sondes, in situ measurements of various organic and inorganic trace species from aircraft, and O_3 column measurements from satellite.

The current study reexamines the influence of biomass burning over the tropical Atlantic domain, as performed previously by *Krishnamurti et al.* [1993, 1996] and *Thompson et al.* [1996a] by different methods. We extend these studies toward higher latitudes in both hemispheres and use our model to quantify the relative contributions by stratosphere-troposphere exchange (STE) and in situ photochemical O_3 formation in the troposphere. We use a coupled chemistry-general circulation model, which calculates background CH_4-CO-NO_x-HO_x tropospheric chemistry and global meteorology on a T30 resolution (3.75° × 3.75°, with a time step of 1800 s) with a direct coupling between chemical and meteorological simulations, for example, of cloud and boundary layer processes. Previously, the performance of the model was evaluated by comparing the simulated tropospheric O_3 climatology with long-term measurements of surface O_3 concentrations, O_3 vertical profiles, and the tropospheric O_3 columns derived from satellite data [*Roelofs and Lelieveld*, 1995, 1997]. In this work we examine the representativeness of the calculated O_3 distributions over the tropical Atlantic Ocean during the biomass burning season and analyze the transports and chemistry simulated by the model. Section 2 gives a brief description of the model. In section 3, calculated O_3 levels are compared with the surface O_3 climatology of *Winkler* [1988], the September/October 1988 latitude-altitude O_3 distribution by *Smit et al.* [1990], and ozone sonde measurements from TRACE A [*Thompson et al.*, 1996a] to validate the model. In section 4, we analyze the influence of the governing horizontal and vertical air motions on O_3 distributions over the (sub) tropical SH Atlantic Ocean and the relative role of STE. Section 5 focuses on O_3 production and destruction in the tropical South Atlantic Ocean region. The conclusions are presented in Section 6.

2. Model Description

The general circulation model (GCM) used in this study is the 19-layer European Center Hamburg Model, version 4 (ECHAM4). In the T30 version, which is used in this study, the horizontal resolution is approximately 3.75° × 3.75°, and the time resolution is 1800 s. The model uses 19 vertical layers in a hybrid σ-p coordinate system, from the surface to 10 hPa. Average pressure levels relevant for the troposphere and lower stratosphere are 990, 970, 950, 900, 840, 760, 670, 580, 490, 400, 320, 250, 190, 140, 100, and 75 hPa, referring to approximate midlayer altitudes of 0.03, 0.14, 0.38, 0.78, 1.4, 2.1, 3.1, 4.2, 5.6, 7.0, 8.6, 10.2, 11.9, 13.8, 15.9, and 18.0 km above the surface, respectively. Tracer transport is calculated using a semi-Lagrangian advection scheme [*Rasch and Williamson*, 1990]. Additional vertical transports are included through parameterizations for vertical diffusion and convection [*Roeckner et al.*, 1996; *Tiedtke*, 1989]. An elaborate description of ECHAM and the simulated climate is given by *Roeckner et al.* [1995], *Chen and Roeckner* [1996], and *Haskins et al.* [1995]. The GCM has previously been used for tracer transport studies [*Feichter et al.*, 1991; *Brost et al.*, 1991] and a simulation of the global sulfur cycle [*Feichter et al.*, 1996]. For this study, it is coupled to a tropospheric chemistry model that considers background CH_4-CO-NO_x-HO_x chemistry, emissions of NO and CO, dry deposition of O_3, NO_2, HNO_3, and H_2O_2, and wet deposition of HNO_3 and H_2O_2. Concentration changes due to chemical reactions are calculated explicitly for all species by means of an Eulerian Backward Iterative (EBI) scheme. A detailed description and analysis of the coupled chemistry GCM is given by *Roelofs and Lelieveld* [1995, 1997].

The model considers a biomass burning source for NO of 6 Tg N yr^{-1} and for CO of 700 Tg CO yr^{-1}, distributed according to *Hao and Liu* [1994]. NO emissions from soils and from lightning play an additional role in the tropical tropospheric O_3 budget. Their respective sources in the model are 5.5 Tg N yr^{-1}, distributed according to *Yienger and Levy* [1995], and 5 Tg N yr^{-1}, parameterized according to *Price and Rind* [1992]. Further, the model considers global NO emissions from fossil fuel burning (21 Tg N yr^{-1} [*Benkovitz et al.*, 1996]), and CO emissions from fossil fuel burning (450 Tg CO yr^{-1}), vegetation (100), formation from natural (280) and anthropogenic (300) higher hydrocarbons, oceans (40), and wildfires (30). CO emissions are distributed according to *Lelieveld and van Dorland* [1995]. Total NO and CO emissions considered in the model are 37.5 Tg N yr^{-1} and 1900 Tg CO yr^{-1}, consistent with *Intergovernmental Panel on Climate Change* (*IPCC*) [1994]. In view of the relatively long lifetime of CH_4 we prescribe CH_4

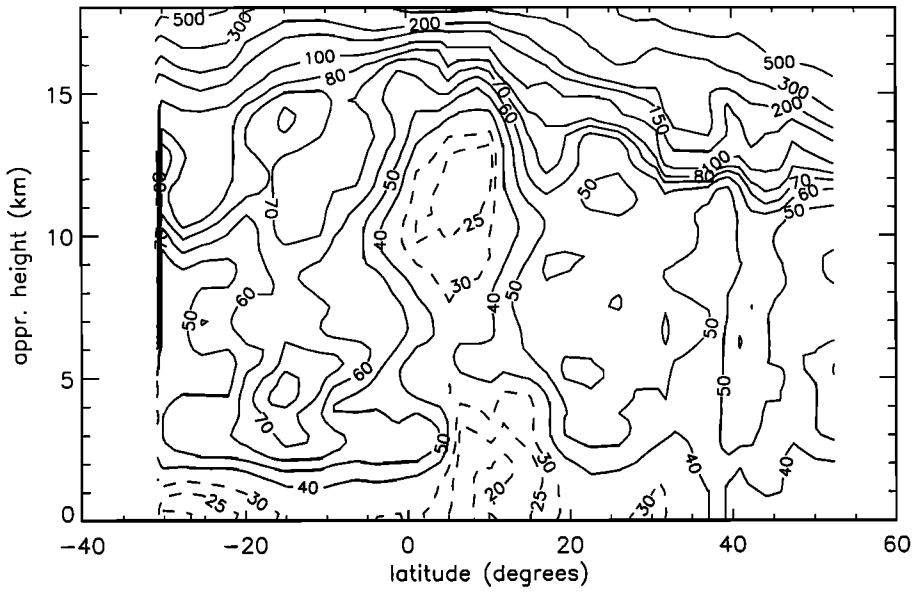

Figure 1. Tropospheric distribution of O_3 mixing ratios (parts per billion by volume (ppbv)) along 30°W, measured aboard the research vessel *Polarstern* in September/October 1988 [*Smit et al.*, 1990, 1991].

surface concentrations of 1772 ppm in the NH and 1680 in the SH [*Lowe et al.*, 1994].

The parameterization for the dry deposition of O_3, NO_x, and HNO_3 is described by *Ganzeveld and Lelieveld* [1995]. It derives aerodynamic and stomatal resistances directly from parameters calculated by ECHAM4. The wet scavenging of HNO_3 and H_2O_2 is calculated using the large scale and convective cloud and precipitation properties calculated on-line by the climate model as described by *Roelofs and Lelieveld* [1995]. Stratospheric O_3 concentrations are prescribed between 1 and 2 model layers above the tropopause up to 10 hPa, the top level of the GCM. Transports of O_3 across the tropopause depend directly on the air motions simulated by the GCM. The simulated tropopause is marked by a potential vorticity of 3.5 10^{-6} K m^2 kg^{-1} s^{-1} poleward of 20° latitude [*Hoerling et al.*, 1993] and by a -2 K km^{-1} temperature lapse rate equatorward of 20° latitude.

Evaluation of the calculated O_3 climatology shows that the model realistically represents the seasonal variability of the O_3 photochemical production and of O_3 transport from the stratosphere. The model successfully reproduces surface O_3 concentration patterns measured in remote and relatively clean conditions but appears to underestimate O_3 concentrations in polluted regions due to the neglect of higher hydrocarbon chemistry [*Roelofs and Lelieveld*, 1997].

Apart from O_3, the chemical model considers a tracer for O_3 that originates from the stratosphere, referred to as O_3s, as described by *Roelofs and Lelieveld* [1997]. In the stratosphere, O_3s is treated in the same way as O_3. It is transported from the stratosphere into the troposphere along with the calculated air motions. In the troposphere, O_3s is subject to photochemical destruction by the same reactions that destroy O_3, that is, with OH, HO_2, and through photodissociation followed by OH production, but not to photochemical production. It is also removed by dry deposition. The difference between the concentrations of O_3 and O_3s is a measure for O_3 that originates from photochemistry in the troposphere, referred to as O_3t. It must be noted that O_3s and O_3t are coupled to a certain degree because other trace gas concentrations and the insolation intensity codetermine the O_3 concentration. STE intensity fluctuations that affect tropospheric O_3s levels directly are partly compensated through photochemical production of O_3t or destruction of O_3s and O_3t. However, the chemical lifetime of O_3 in the troposphere varies between a few days in the lower tropical troposphere and a few weeks to a few months in high latitudes. This is generally longer than the timescales of transport processes in the troposphere, which are of the order of hours, for example, for convection, to a week for synoptic scale disturbances. Thus modeled O_3, O_3s, and O_3t fields provide an appropriate analytical tool to assess the influence of chemistry and transports within the troposphere and between the stratosphere and the troposphere.

The specific contribution of biomass burning emissions on tropospheric O_3 cannot be calculated directly because the model does not consider separate emission sources in the photochemical calculations. However, biomass burning contributes more than 80% of the total NO emissions in the tropical Atlantic region in the dry season, while the remainder is largely due to natural sources, that is, soils and lightning. Biomass burning therefore dominates photochemical O_3 production in the region of interest.

3. Comparison of Simulated and Measured O_3

3.1. Comparison of Model Results and Ship Cruise Measurements

A total of 40 ozone soundings were launched on a ship cruise from Bremerhaven, Germany (53°N), to Rio Grande del Sol, Brazil (32°S), between September 15 and October 9, 1988, with a latitudinal resolution between 1.5° and 2.5°. Figure 1 shows the measured latitudinal and vertical distribution of tropospheric O_3 [*Smit et al.*, 1990, 1991], processed with an improved background signal correction [*Smit et al.*, 1994].

The measurements show a column of O_3-low air around 10°N, where the intertropical convergence zone (ITCZ) is located. Similar low-O_3 areas are found in the tropical Indian

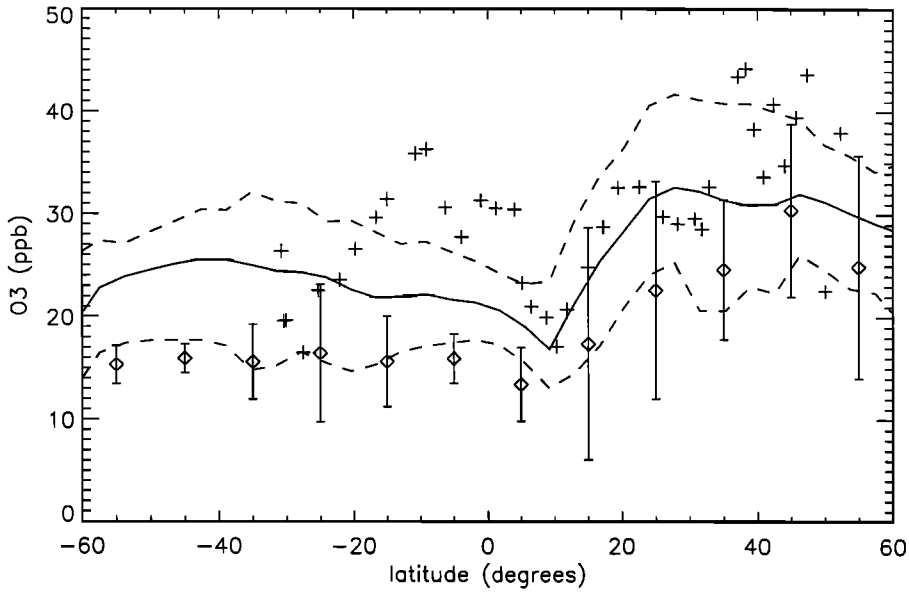

Figure 2. Surface O_3 mixing ratios (ppbv) along 30°W derived from ozone sondes [*Smit et al.*, 1990, 1991] (plusses), from the climatology of *Winkler* [1988] (diamonds, bars represent 2 standard deviations), and simulated by the model for September/October (solid line, dotted lines represent 2 standard deviations).

and Pacific Oceans [e.g., *Fishman et al.*, 1990]. Photochemical destruction of O_3 prevails at the ocean surface due to high insolation and high water vapor concentrations. Convection, connected with the upward branch of the Hadley circulation, efficiently transports the O_3-depleted air upward. The tropical tropopause is located at approximately 16 km altitude, and the subtropical tropopause "breaks" can be identified at about 20°–30° latitude in both hemispheres [*Smit et al.*, 1990]. The NH and SH subtropical regions are characterized by downward transport of O_3-rich air from the upper troposphere. The areas of relatively high O_3 between 10 and 13 km at 15°–5°S, between 6 and 12 km at 20°N, and between 5 and 10 km at 45° are characterized by relatively low water vapor concentrations, which indicates that the air may have originated from the stratosphere [*Smit et al.*, 1990]. On the other hand, the O_3 high between 5° and 20°S in the lower troposphere is believed to originate from photochemical production associated with biomass burning emissions. This is also suggested by enhanced surface concentrations of nonmethane hydrocarbons and HNO_3, measured on the same cruise [*Koppmann et al.*, 1992; *Papenbrock et al.*, 1992].

Qualitatively, the distribution in Figure 1 is highly similar to climatological, zonally averaged O_3 distributions that result from model simulations [*Roelofs and Lelieveld*, 1995; *World Meteorological Organization (WMO)*, 1995] or from a compilation of observations [*Crutzen*, 1995]. Nevertheless, it must be kept in mind that Figure 1 refers to an instantaneous distribution, with influences from instantaneous wind fields, the location and intensity of the ITCZ, and changes of synoptic scale characteristics between soundings, which characterize a specific meteorological situation at the time of the cruise. The potential variability of O_3 over the middle Atlantic Ocean is illustrated by comparing Figure 1 with similar distributions measured on ship cruises [*Smit et al.*, 1991; *Weller et al.*, 1996].

The model simulations do not describe a particular year but rather an "average" meteorology. Therefore a direct comparison of the measured distribution with model results is of limited use. Instead, we use model results for September and October of 2 subsequent model years and include the modeled variability of O_3 mixing ratios in the comparison. Figure 2 shows calculated surface O_3 mixing ratios for 30°W, averaged over the 2 × 2 months. The model variability is indicated by the standard deviation. Also shown are the Atlantic Ocean surface O_3 climatology, averaged over September and October and including the standard deviation, obtained by *Winkler* [1988], and the surface mixing ratios derived from the individual vertical profiles obtained during the *Polarstern* cruise [*Smit et al.*, 1990].

For NH (sub) tropical latitudes there is good agreement between the calculated and the *Polarstern* surface concentrations. The model somewhat underestimates O_3 at middle and higher latitudes. The O_3 minimum near 10°N matches the observations, indicating that the location of the ITCZ is simulated accurately. A major discrepancy is found in the SH tropics, where the *Polarstern* measurements indicate a distinct local surface O_3 maximum of about 35 parts per billion by volume (ppbv) at 10°S, attributed to biomass burning activities. The model does not capture this feature. Qualitatively, the calculated O_3 surface distribution agrees relatively well with the surface O_3 climatology of *Winkler* [1988], with highest concentrations in the NH, a minimum around 10°N connected with the ITCZ, and higher concentrations again in the SH. However, the calculated values are systematically about 5 ppbv higher, and the simulated variability is smaller than measured in the NH and larger in the SH. Note that the *Polarstern* measurements in the NH are also relatively high compared to the distribution of *Winkler* [1988]. Ozone increases over Europe and the eastern United States have been relatively small since 1980, that is, over the period between these measurements [*Logan*, 1994]. Therefore the differences probably do not result from increased anthropogenic emissions of O_3 precursors from adjacent continents. An explanation may be that the *Winkler* [1988] measurements were not subject to absolute calibration and a systematic offset cannot be ruled out.

Figure 3 shows the simulated and measured latitudinal O_3 distribution at selected altitudes. The simulated temporal vari-

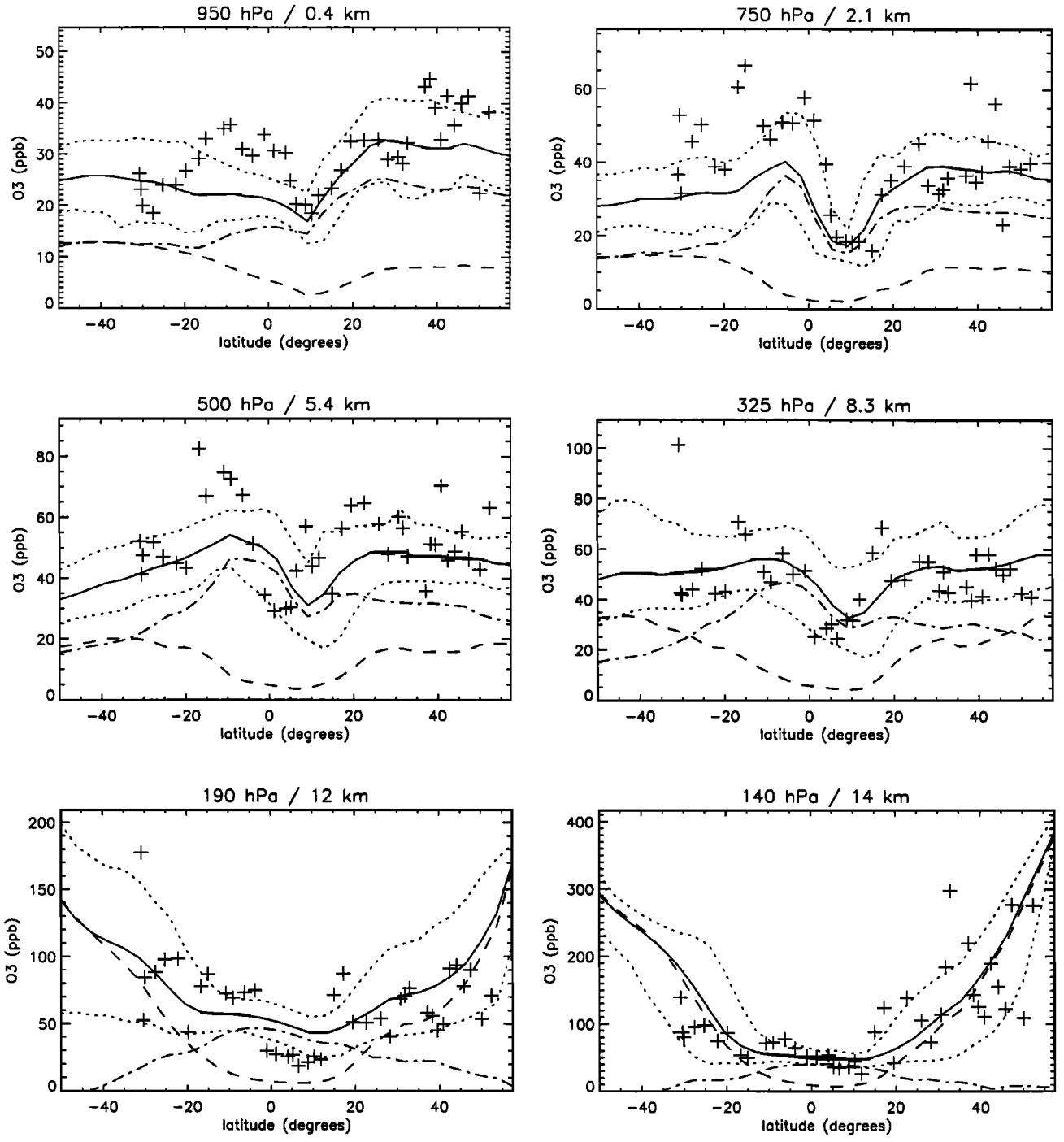

Figure 3. O_3 mixing ratios (ppbv) at selected altitudes along 30°W from ozone sondes [*Smit et al.*, 1990, 1991] (plusses) and simulated by the model for September/October (solid lines, dotted lines represent the 90-percentile interval). Also shown are the contributions by O_3s (dashed lines) and O_3t (dash-dotted lines).

ability is illustrated by the 90-percentile range. The figure also shows the average contributions of photochemically produced O_3 (O_3t) and O_3 of stratospheric origin (O_3s). The 90-percentile range of the modeled O_3 agrees reasonably well with the measured concentrations and their inherent variability throughout the NH and in the middle and upper SH troposphere, as well as in the lower stratosphere at middle latitudes. However, a significant discrepancy between model and measurements exists for the SH lower troposphere below 6 km. The observed O_3 maximum between approximately 0° and 30°S is only partly captured by the model at 2.1 and 5.4 km and not at all at lower altitudes (cf. Figure 2). Our results indicate that O_3 from the stratosphere (dashed lines) is relatively unimportant in this region compared to photochemically produced O_3 (dash-dotted lines in Figure 3). In the lower tropical troposphere, high insolation and water vapor concentrations lead to efficient photochemical destruction of O_3 from the stratosphere, while relatively high O_3 levels are photochemically produced as a result of biomass burning emissions. From this we conclude that the O_3 underestimation by the model results

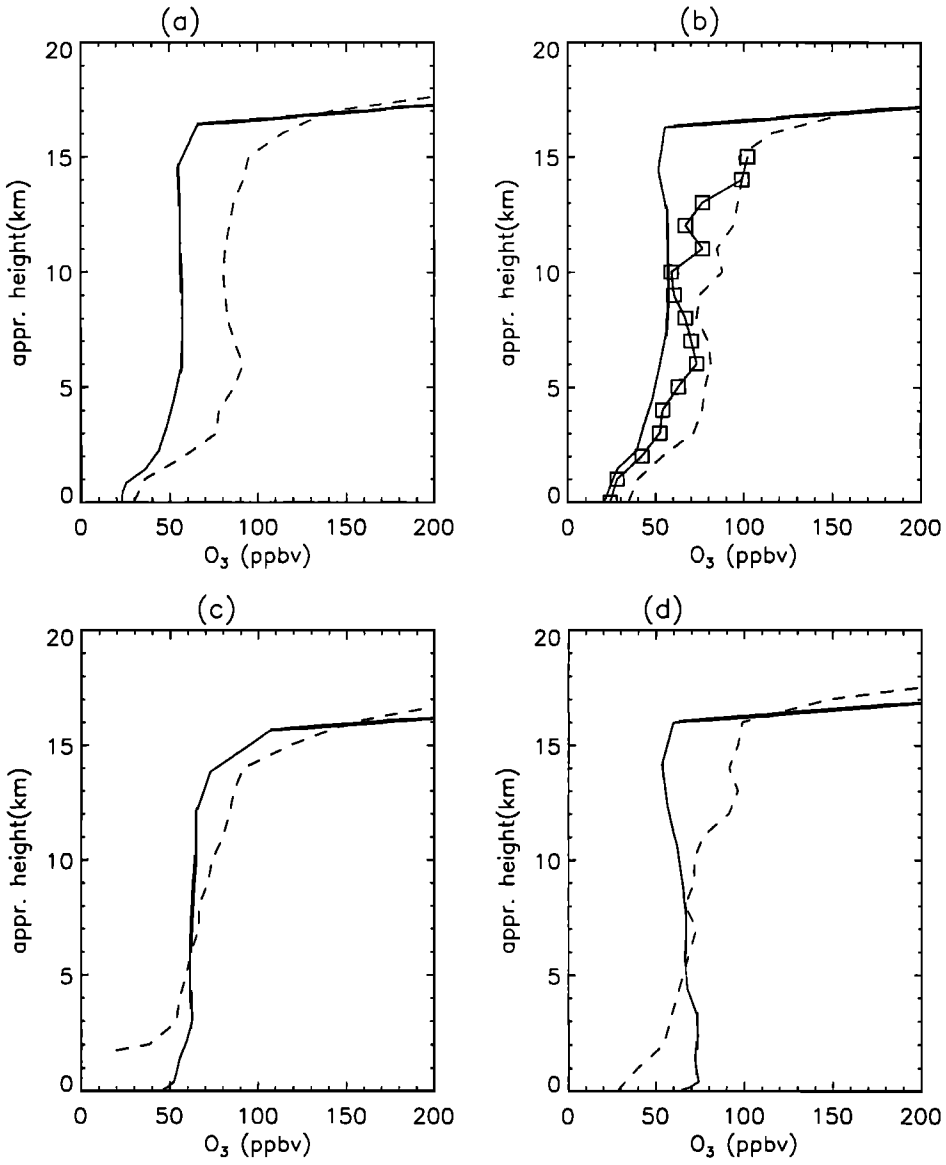

Figure 4. Simulated O_3 (ppbv) for grid cells representing (a) Ascencion Island (8°S, 14°W), (b) Natal, Brazil (5°S, 35°W), (c) Irene, South Africa (26°S, 28°E), and (d) Brazzaville, Congo (4°S, 15°E). Vertical O_3 profiles measured during TRACE A [*Kirchhoff et al.*, 1996; *Diab et al.*, 1996; *Thompson et al.*, 1996a] are given by the dashed lines; the Natal September climatological average is denoted by squares [*Kirchhoff et al.*, 1996].

from inefficient photochemical buildup from biomass burning emissions, rather than from an underestimation of STE. A significant part of biomass burning emissions consists of nonmethane hydrocarbons [e.g., *Crutzen*, 1995; *Talbot et al.*, 1996] which enhance photochemical O_3 production, whereas the model only considers background CH_4-CO-NO_x-HO_x chemistry. However, it cannot be ruled out that specific meteorological conditions have influenced the measured O_3 distribution in the lower troposphere, which have not been captured by our climate model. Regional transport and mixing processes may improve by applying dynamical adjustment techniques on the basis of ECMWF-analyzed meteorology [*Jeuken et al.*, 1996], which we have planned for the future. In section 4 the transport patterns simulated by the GCM will be analyzed in more detail.

Between 0° and 10°N the model overpredicts O_3 at 12 km. This is the region of the ITCZ, characterized by upward convective transports. The model results indicate that photochemically produced O_3 dominates here over O_3 from the stratosphere. At this altitude the model vertical resolution is relatively low (2 km around the tropical tropopause), resulting in less accurate chemical transports and artificially enhanced vertical mixing of O_3 precursors. Further, the effect of heterogeneous photochemical destruction of O_3, not considered by the model, may be significant in the tropics [*Lelieveld and Crutzen*, 1990]. On the other hand, just below the tropopause at 14 km, the agreement between measured and modeled concentrations is good. In the NH lower troposphere in the vicinity of 40°N the underestimation of modeled O_3 may be related to the neglect of higher hydrocarbon chemistry, although the effect seems to be smaller compared to the biomass burning plume, as discussed earlier. It must be noted that north of 40°N the *Polarstern* route curves toward the European continent and thus it is closer to the pollutant sources where O_3 concentrations are higher.

3.2. Comparison of Modeled O_3 and SAFARI/TRACE A Measurements

Figure 4 shows simulated vertical O_3 concentration profiles for four locations in the SH Atlantic Ocean region, averaged over the 2 × 2 months. The figure also shows average profiles measured during SAFARI/TRACE A [from *Kirchhoff et al.*, 1996; *Diab et al.*, 1996; *Thompson et al.*, 1996a]. The model appears to underestimate O_3 at Ascencion and Natal. Qualitatively, the gradient between the surface and 2 km altitude of the Ascencion and Natal vertical profiles is captured by the model. At Ascencion the model reproduces the O_3 maximum between 2 and 7 km altitude, associated with westward transport of air from African biomass burning regions, and somewhat lower concentrations in the upper troposphere, associated with advection from South American biomass burning areas (transports will be discussed in section 4.2). However, absolute O_3 concentrations are underestimated by 20–40 ppbv throughout the troposphere. It should be noted that satellite-derived O_3 columns at Ascencion and Natal measured during TRACE A are significantly larger than climatological O_3 columns [*Fishman et al.*, 1996b], indicating that 1992 was anomalous in this respect. Also, vertical O_3 profiles measured at Natal during TRACE A show significantly higher concentrations than the Natal September climatological average, as shown by the squares in Figure 4 [*Kirchhoff et al.*, 1996]. This is probably due to an unusually active period for convection and upper tropospheric O_3 formation [*Pickering et al.*, 1996; *Kirchhoff et al.*, 1996]. Owing to the relatively coarse model resolution, the local orography at Irene is not well represented in the model. The vertical concentration gradient in the model at Irene is weaker than measured, leading to an underestimation of the O_3 levels in the middle and upper troposphere. We calculate a negative O_3 lapse rate at Brazzaville, in contrast to the measured profiles. This may be due to specific local, subgrid scale conditions (e.g., convection) that are not captured by the model. The model grid representing Brazzaville is located at the African continental outflow region, where convective transports do not penetrate the upper troposphere (section 4.2). Overall, the model somewhat underestimates the tropospheric O_3 column, while the tropopause heights are represented relatively well at these sites.

4. Modeled O_3 Distribution Over the Southern Atlantic Ocean

4.1. Distribution of O_3

Figure 5 shows the simulated tropospheric O_3 columns (DU) over the (sub) tropical Atlantic region, averaged over (two times) September and October. Also shown are the contributions of O_3 from the stratosphere (O_3s) and O_3 that is photochemically produced in the troposphere (O_3t). In this section we will shortly describe the calculated distributions; a comparison with satellite data [*Fishman et al.*, 1990; *Hudson et al.*, 1995] is presented by *Roelofs and Lelieveld* [1997].

Stratospheric O_3 enters the troposphere at middle and high latitudes through tropopause foldings connected with synoptic scale disturbances and through transports along isentropic surfaces [e.g., *Holton et al.*, 1995]. O_3s columns are smaller in the NH in September/October (Figure 5b) because cross-tropopause transports of O_3 minimize in the autumn [*Roelofs and Lelieveld*, 1997]. Between 5°S and 15°N the contribution of O_3s to total O_3 is at minimum (<5 DU) because local down-

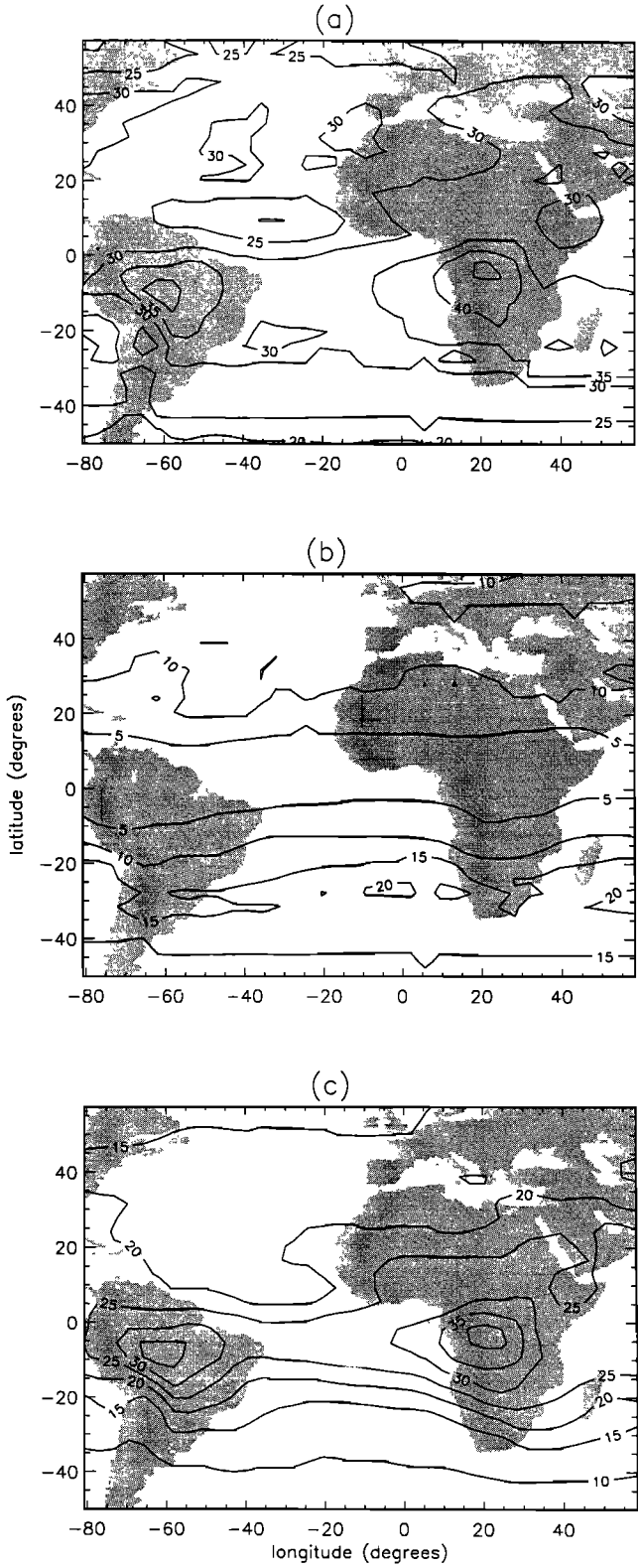

Figure 5. Simulated tropospheric columns (Dobson units (DU)) over the Atlantic Ocean and adjacent continents of (a) total O_3, (b) O_3s, and (c) O_3t, averaged over September/October.

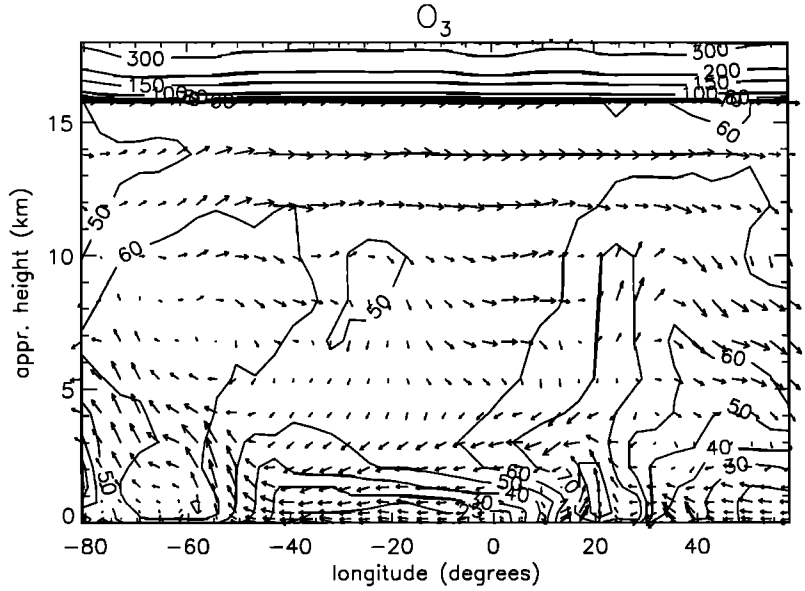

Figure 6. Longitudinal cross section of simulated O_3 mixing ratios (ppbv) for the month September at approximately 6°S. Also shown are the simulated wind fields (arrow length in arbitrary units).

ward transport from the stratosphere is insignificant and photochemical destruction is efficient. In September and October, the dry season, biomass burning is at its maximum in the SH. Large amounts of photochemically produced O_3 prevail over the Atlantic Ocean around 5°S latitude, an area where biomass burning emissions from South America and Africa converge (Figure 5c). Transport to the Indian Ocean region of O_3 from African biomass burning areas also appears to be significant. Southward of 20°S, total O_3 columns decrease as the influence of O_3t, the principal O_3 component in the tropics, decreases. However, O_3s becomes increasingly important and dominates poleward of 30°S. Over the ocean at about 10°N, O_3 columns are relatively low, associated with efficient photochemical destruction in the ITCZ. In middle latitudes in the NH, relatively large amounts of O_3t are found, but longitudinal differences are much smaller compared to the SH.

4.2. Transports of O_3 Over the Tropical South Atlantic Ocean

In this section we analyze the simulated atmospheric wind fields in the considered region and their impact on the distributions of O_3 from the stratosphere and the troposphere. The distributions shown in this section and in section 5 display O_3 concentrations and wind vectors that are averaged over the second half of September of the second simulated year. We emphasize that simulated instantaneous wind fields and O_3 distributions are characterized by relatively high temporal and spatial variability due to synoptic scale features, as is illustrated in Figure 3. The averaging is applied in order to reduce the day-to-day variability of the calculated wind fields and O_3 distributions. The averaged fields illustrate transport and O_3 patterns on a timescale which is representative for the large scale transports in the South Atlantic Ocean region. For example, in the latitude band 0°–10°S, lower tropospheric transports from the African (20°E) to the South American (40°W) continent take place on a timescale of 5–10 days [e.g., *Thompson et al.*, 1996b, Plate 1].

Figure 6 shows the longitudinal distribution of O_3 along 6°S, the latitude where photochemical O_3 columns (O_3t) maximize (Figure 5c). The stratospheric O_3 component is relatively small near the equator; O_3 levels are dominated by photochemical formation in the troposphere, mostly due to biomass burning. Therefore the separate O_3s and O_3t distributions are not shown. Vertical winds in Figure 6 represent large scale rising and sinking motions, not the individual convective updrafts and associated downdrafts. Between 15° and 20°E, over the African continent, the model simulates an inversion layer at an altitude of about 3 km, where O_3 convergence takes place at the top of the boundary layer. Easterly advection transports O_3-rich air from Africa over the Atlantic Ocean at about 3–4 km altitude. Near the west coast of Africa, at about 15°E, the simulated vertical profile resembles the vertical distribution of O_3 measured in Congo during the dry season, which shows relatively high O_3 concentrations between 1 and 4 km altitude [*Crutzen and Andreae*, 1990].

Between 60° and 70°W, over South America, O_3 levels are relatively high in the lower troposphere (up to 80 ppbv). This O_3 is advected upward relatively efficiently up to about 12 km altitude. The O_3 precursors NO_x and CO, not shown here, are also transported upward. The model simulates NO_x levels between about 100 and 500 parts per trillion by volume (pptv) between the boundary layer and 10 km altitude, as will be discussed in section 5. These concentrations suffice to cause significant additional photochemical production of O_3 in the free troposphere. At high altitudes, westerly wind carries O_3 from South America over the ocean toward Africa. Further, air motions between 5 and 10 km altitude over eastern Africa efficiently transport O_3 precursors and photochemically produced O_3 eastward, leading to a band of relatively high column O_3 between 10° and 30°S over the Indian Ocean [*Fishman et al.*, 1990; *Roelofs and Lelieveld*, 1997]. The simulated low-level flow from the African continent and eastward transports at higher altitudes from the South American continent resemble the October 1989 meteorology in the region presented by *Krishnamurti et al.* [1993] and agree well with the trajectory

analyses of SAFARI/TRACE A [*Thompson et al.*, 1996a]. The simulated marine lower troposphere is characterized by a relatively strong vertical gradient of O_3, with mixing ratios up to 70 ppbv at about 3 km altitude and 25 ppbv at the surface. The latter is associated with southeasterly transports of boundary layer air (of which Figure 6 shows the westward component) from middle latitudes toward the ITCZ, characterized by relatively low O_3 levels.

Figure 7 shows latitude-altitude distributions of O_3, O_3s, and O_3t over the central Atlantic Ocean along 30°W. The large scale wind pattern clearly signifies the Hadley circulation and its impact on the O_3 distribution. A relatively O_3-poor column of air is simulated at 10°N, where the ITCZ is located. The combination of high insolation and high water vapor concentrations leads to efficient photochemical destruction of O_3 near the ocean surface, mainly through photodissociation of O_3 and subsequent reaction of $O(^1D)$ with water vapor. Convection at the ITCZ efficiently transports the O_3-depleted surface air upward to the middle and upper troposphere. Downward transports of relatively O_3-rich air, mostly originating from the stratosphere, occur north and south of the ITCZ between 20° and 40° latitude. O_3 from photochemical production is abundant between the SH middle latitudes and the equator, largely due to biomass burning emissions, and throughout the NH, largely due to industrial emissions. The SH Hadley circulation includes surface winds toward the ITCZ, which carry O_3-poor air, whereas the overlying layer is polluted by O_3 from the African biomass burning regions. Mixing between both layers appears to be relatively inefficient, resulting in a strong stratification of O_3 levels in the Atlantic lower troposphere. This agrees with the O_3 concentration profiles measured at Ascension Island (8°S, 15°W), which show O_3 mixing ratios of about 25 ppbv at the surface up to 70 ppbv at 3 km altitude [*Thompson et al.*, 1996a]. In the NH lower troposphere the simulated vertical O_3 concentration gradient is smaller than in the SH, as is also apparent from observations [*Smit et al.*, 1990; *Weller et al.*, 1996].

Finally, Figures 8 and 9 display horizontal wind fields and O_3, O_3s, and O_3t distributions for approximate altitudes of 2.1 km (750 hPa) and 6.8 km (400 hPa). At 2.1 km (Figure 8), easterly flow from the African continent is associated with relatively high O_3 mixing ratios. This flow influences O_3 levels over Ascension Island and even over South America [cf. *Fishman et al.*, 1991; *Logan and Kirchhoff*, 1986; *Thompson et al.*, 1996a]. On the other hand, O_3-rich air from the South American biomass burning regions is transported to the southeast, under the influence of a subtropical anticyclone. The anticyclone develops near the South American east coast and then traverses the ocean toward Africa approximately along 25°S. Because Figure 8 displays 2-weekly averaged wind fields, this appears as an extended band between both continents. In the (sub) tropical areas the stratospheric O_3 component generally contributes less than 10% to the calculated O_3 levels (Figure 8b). Consequently, O_3 from photochemical production (O_3t) dominates the (sub) tropical O_3 distribution (Figure 8c). In the SH middle latitudes the model calculates surface O_3s mixing ratios above 15 ppbv, which contributes about 30–50% to surface O_3 levels. At 6.8 km altitude (Figure 9), westerlies dominate in the SH. At (sub) tropical latitudes, these winds carry relatively O_3-rich air from South America toward Africa. Figure 9c shows that this O_3 originates predominantly from photochemical production. However, between 20° and 40°S, relatively large O_3s abundances are simulated, indicating relatively efficient STE in this region. Here O_3 from the stratosphere contributes significantly to total O_3 levels.

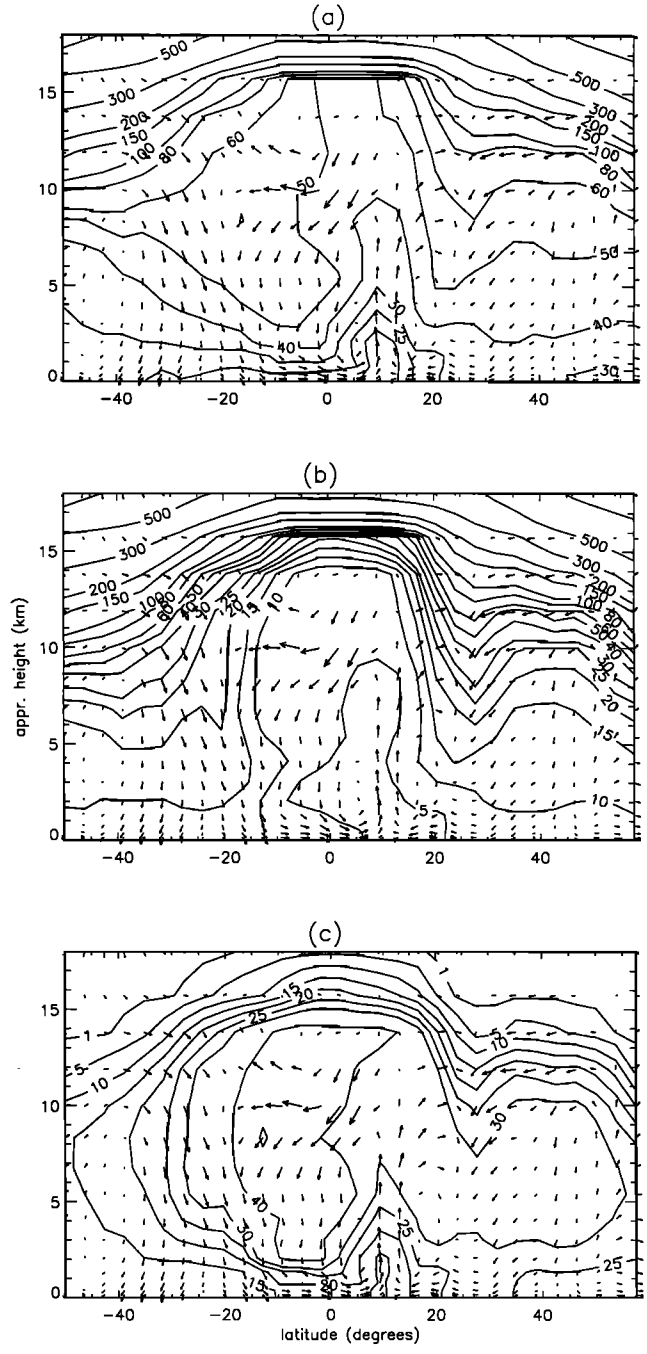

Figure 7. Latitudinal cross section of simulated mixing ratios (ppbv) for (a) total O_3, (b) O_3s, and (c) O_3t for the month September at approximately 30°W. Also shown are the simulated wind fields (arrow length in arbitrary units).

5. Photochemical O_3 Production and Destruction

Figure 10 shows the longitudinal distribution of the calculated net O_3 production/destruction rate along 6°S, coincident with the O_3 distribution in Figure 6. The model simulates relatively strong net O_3 production over South America and Africa, from about 50 ppbv d^{-1} near the surface to 4 ppbv d^{-1}

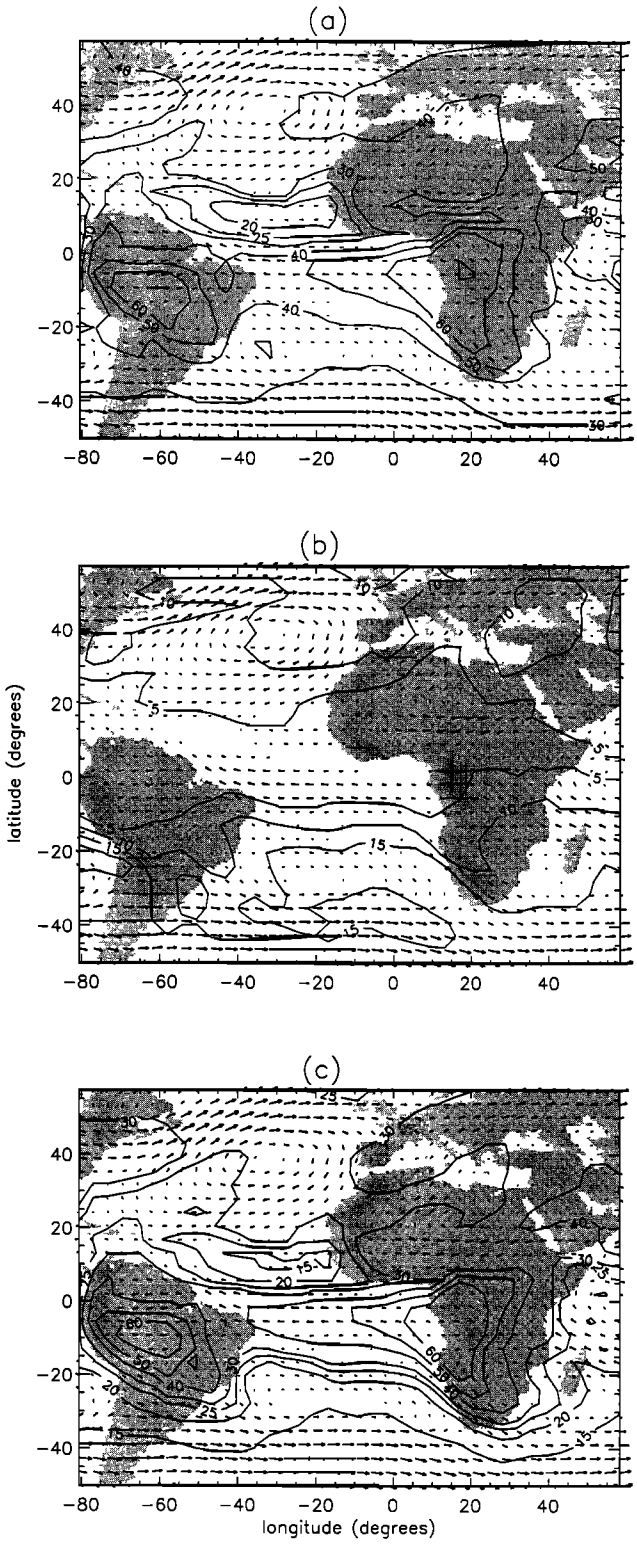

Figure 8. Simulated mixing ratios (ppbv) for (a) total O_3, (b) O_3s, and (c) O_3t for the month September at an altitude of 2.1 km (750 hPa). Also shown are the simulated wind fields (arrow length in arbitrary units).

between 8 and 12 km altitude. The upper tropospheric O_3 production rates result from convective activity in the region, which vertically redistributes surface emitted pollutants. *Pickering et al.* [1996] calculate an O_3 production rate up to 7–8 ppbv d^{-1} in convective outflow. Note that this cannot be directly compared to our results because of the subgrid scale representation of convection in the climate model. Lightning emissions of NO may add significantly to O_3 production in the free troposphere [e.g., *Levy et al.*, 1996; *Pickering et al.*, 1996]. Destruction of O_3 dominates over the Atlantic Ocean in the lower troposphere. Destruction is most efficient near the ocean

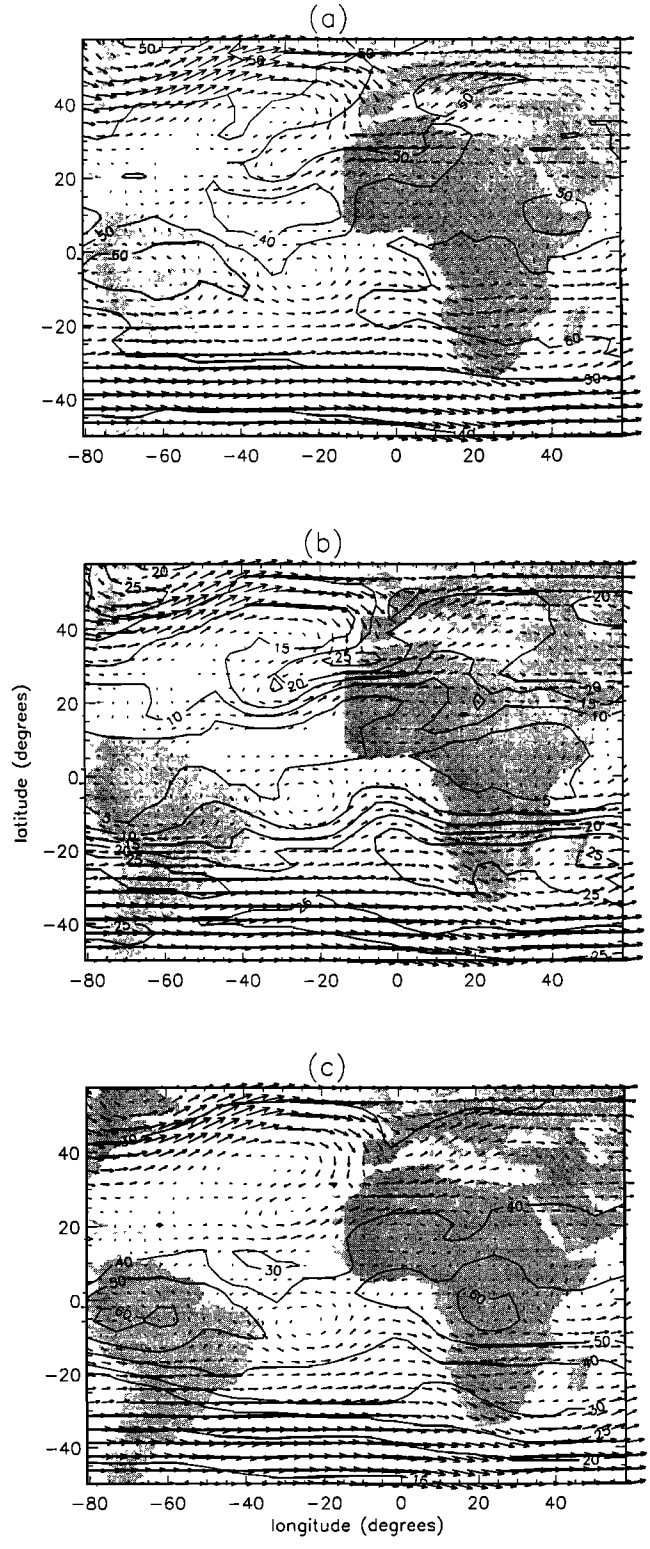

Figure 9. As in Figure 7, but for 6.8 km altitude (400 hPa).

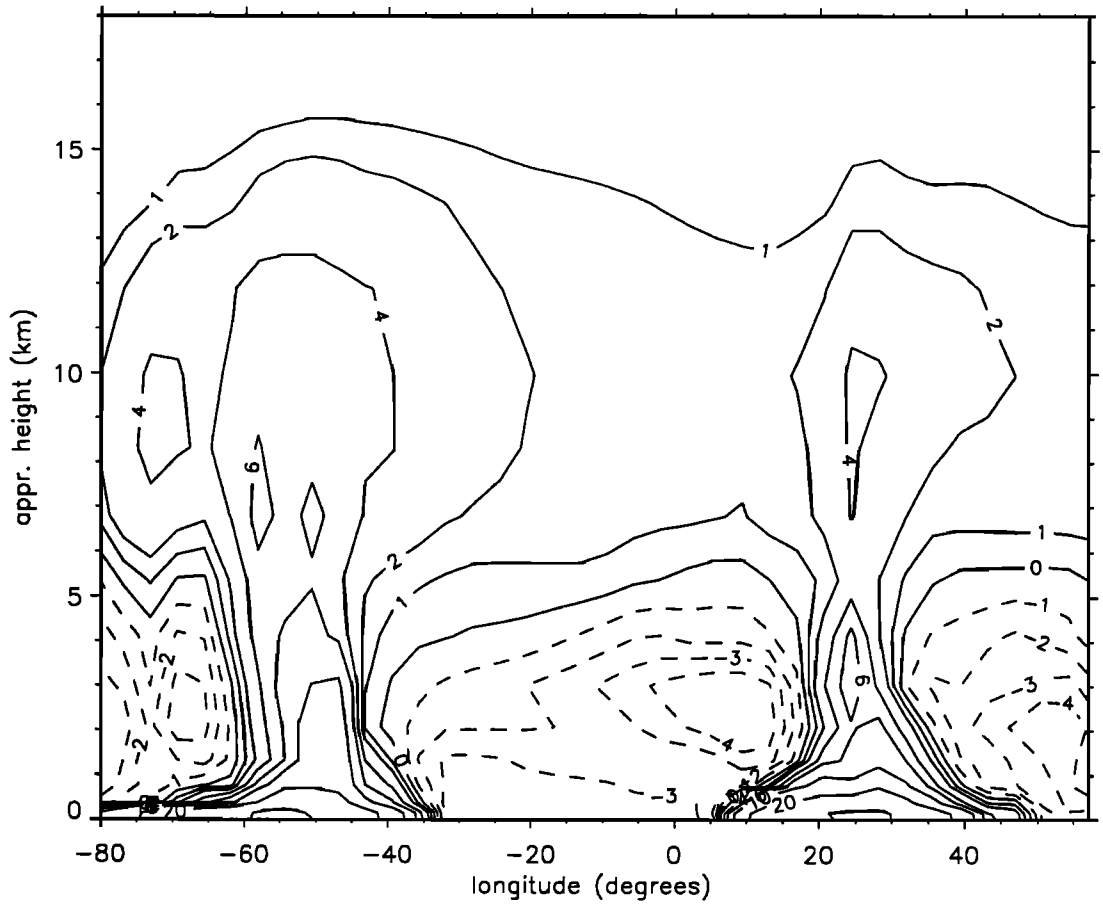

Figure 10. Longitudinal cross section of simulated O_3 production/destruction rates (ppbv d^{-1}) for the month September at approximately 6°S. The net photochemical production/destruction rate is the difference between O_3 production through reactions of NO with HO_2 and with CH_3O_2 (higher hydrocarbon chemistry is neglected in the model) and O_3 destruction through reactions of O_3 with OH and with HO_2 and of $O(^1D)$ with water vapor, averaged over 2 weeks.

surface, where water vapor concentrations are high. In addition, at 10°E, at about 2.5 km altitude, O_3 levels are high (Figure 6), and NO_x is rapidly depleted during transport, giving rise to a local O_3 destruction maximum. Figure 11 shows latitudinal distributions of the O_3 precursors NO_x and CO. It can be seen that NO_x mixing ratios decrease from more than 200 pptv over Africa to 10–100 pptv over the ocean. The model simulates rapid conversion from NO_x to HNO_3 in the African outflow region, where HNO_3 mixing ratios up to 2000 pptv are calculated. Although measurements during TRACE A indicate lower HNO_3 levels, between 150–1000 pptv, peroxyacetylnitrate (PAN) ranges between 10 and 1500 pptv, so that measured NO_y concentrations are between 200 and 2100 pptv [*Talbot et al.*, 1996]. This is comparable to the NO_y simulated in the outflow region, to which HNO_3 contributes over 95% (note that PAN is neglected in our model). In the outflow region, CO levels decrease from over 500 ppbv over the continent to about 150 ppbv at 40°W. Although we do not discuss simulated NO_x and CO distributions in detail, we emphasize that the distributions displayed in Figure 11 agree relatively well with data presented by *Jacob et al.* [1996, Plate 2], *Talbot et al.* [1996], and *Connors and Reichle* [1996]. Hence NO_x concentrations decrease strongly during transport from the sources, so that steep gradients between O_3 production and destruction regions develop. Similar gradients occur over the South American west coast and the African east coast, whereas they diminish at altitudes above 5 km. Here air originating from South American biomass burning areas is transported eastward (Figures 6 and 9). O_3 production and loss rates, which have been derived from TRACE A measurements, follow similar patterns. For the South Atlantic basin, *Thompson et al.* [1996a] calculated a net O_3 production/loss between −2.6 and −6 ppbv d^{-1} at 0–4 km, between −0.6 and +1.6 ppbv d^{-1} at 4–8 km, and between 1.5 and 2.6 ppbv d^{-1} at 8–12 km. For the same layers, *Jacob et al.* [1996, Plate 1b] calculated about −1 to −5, 0 to 3, and higher than 2 ppbv d^{-1}, respectively. It should be noted that TRACE A measurements were carried out mostly between 10° and 20°S. The simulated vertical distribution of O_3 production/destruction is similar at these latitudes, but the net production/destruction rates are somewhat lower than at 6°S. The simulated values are therefore rather low compared to the TRACE A analyses. However, the calculated rates are averaged over 2 weeks. Instantaneous noontime production/destruction rates simulated by the model are 100 to 200 ppbv d^{-1} in the continental surface layer, −4 to −8 ppbv d^{-1} in the outflow regions and near the ocean surface, and they exceed 4 ppbv d^{-1} in the upper troposphere over the ocean.

Figure 12 shows calculated O_3 production/destruction rates, integrated over the troposphere. Net O_3 production is limited to the continents, where it exceeds 6 DU d^{-1}. Net destruction

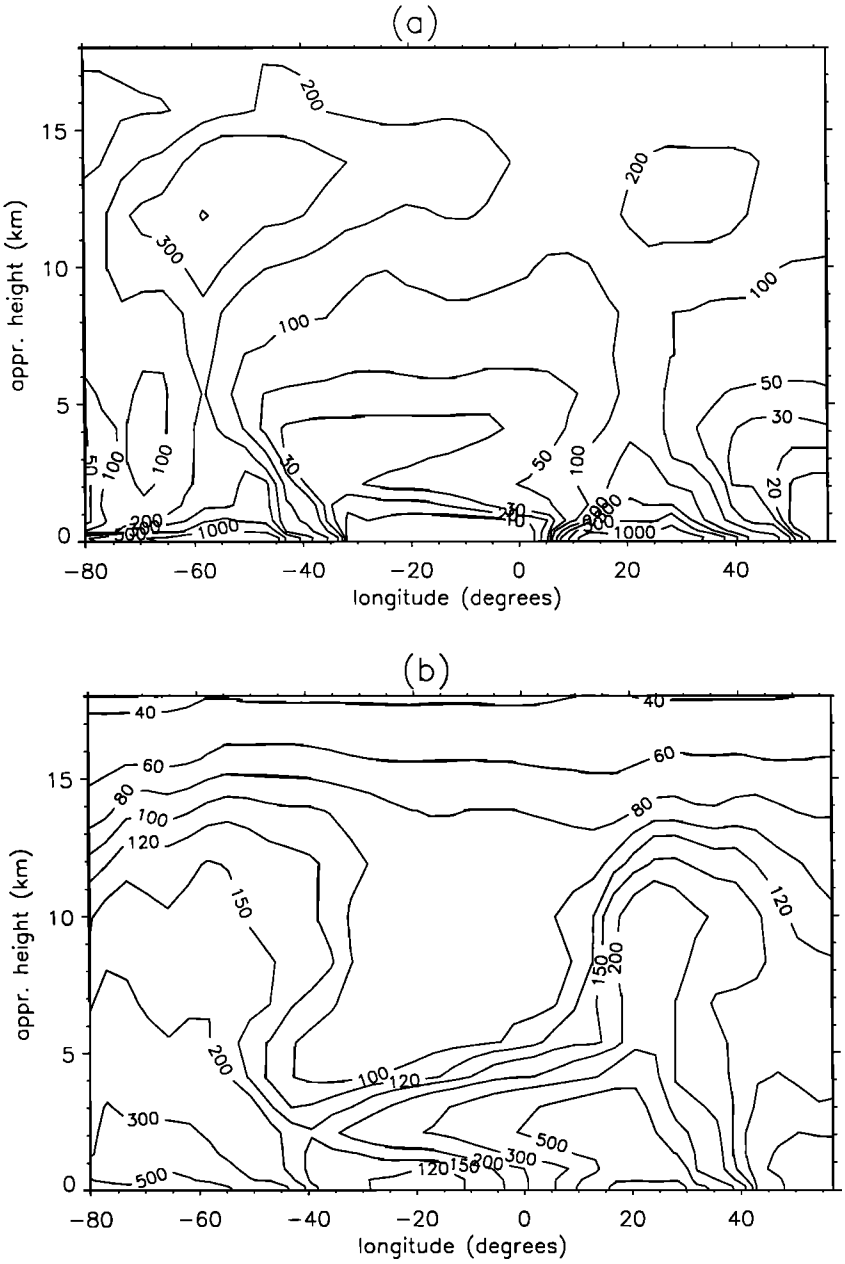

Figure 11. Longitudinal cross section of simulated (a) NO_x (parts per trillion by volume (pptv)) and (b) CO (ppbv) for the month September at approximately 6°S.

prevails over the oceans. At the ITCZ, between 10° and 20°N, net O_3 loss rates of 0.5–1.0 DU d^{-1} are calculated, corresponding with a relative O_3 column decrease of 3–4% d^{-1} (cf. Figure 5). In the South Atlantic Ocean the model simulates efficient O_3 destruction near the central African west coast, coinciding with the African outflow region (approximately 1 DU d^{-1}; 2% d^{-1}), and near 20°S latitude, where lower tropospheric air originating from South American biomass burning areas is transported eastward (Figure 8) (0.3–0.5 DU d^{-1}; 1–2% d^{-1}). Total tropospheric column-integrated O_3 production/loss rates are dominated by the chemistry in the lowest 4 km. For the column between 4 and 12 km the model simulates a net production up to 0.5 DU d^{-1} over the (sub) tropical Atlantic Ocean and up to 1 DU d^{-1} over the continents. Modeled distributions of the column production/destruction rates over the ocean agree reasonably well with O_3 destruction rates derived from TRACE A measurements, which range between −1.3 and −0.2 DU d^{-1} [*Thompson et al.*, 1996a]. However, in contrast with the model results, two TRACE A flights indicated a net O_3 production of about 0.5 DU d^{-1} over the ocean near the west coast of central Africa. Further, TOMS O_3 data suggest a net production of 0.85–2.2 DU d^{-1} during transport from Brazzaville to Ascencion [*Thompson et al.*, 1996b], which is directly over the African outflow region.

6. Conclusions

We have applied our chemistry-climate model to analyze the influence of transports on the O_3 distribution over the SH (sub) tropical Atlantic Ocean. In this region, photochemically

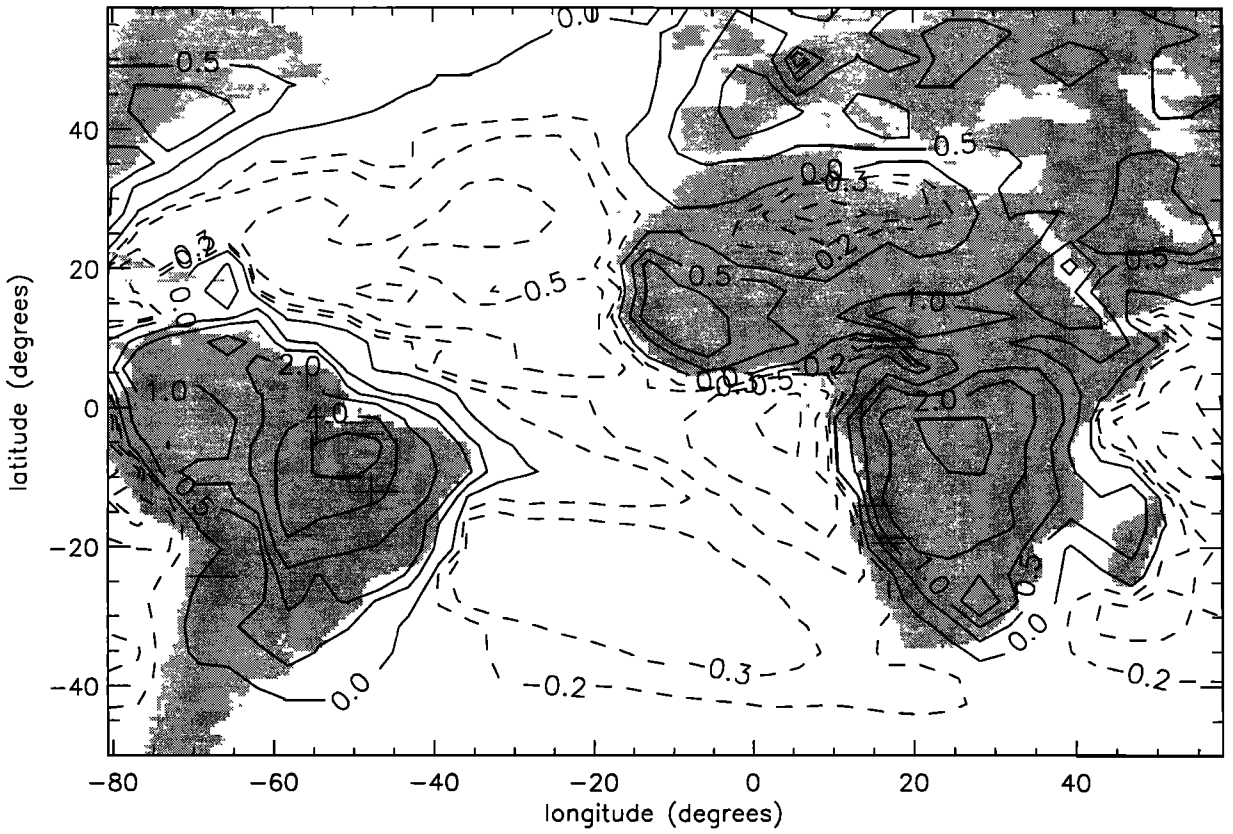

Figure 12. Simulated column-integrated O_3 production/destruction rate (DU d^{-1}) for the month September.

produced O_3 is largely associated with biomass burning emissions which maximize in September/October, the dry season in the SH. The model results show that in the boundary layer, relatively unpolluted marine air is transported from the southeast. Above the boundary layer, between approximately 2 and 5 km altitude, relatively O_3-rich air is transported into the region from the east where the African biomass burning regions are located. Above 5 km, O_3 levels are influenced by westerlies which advect air from the South American biomass burning regions. The model simulates average O_3 production rates of 10–50 ppbv O_3 d^{-1} in the lower troposphere over the biomass burning regions and lower production rates, up to 3 ppbv O_3 d^{-1}, in the middle and upper troposphere. Photochemical destruction of O_3 prevails over the ocean in the lower troposphere, maximizing in the African and South American outflow regions. Between 0° and 20°S, tropospheric O_3 levels are dominated by photochemically produced O_3, while transport of O_3 from the stratosphere is of minor importance. However, between 20° and 30°S, about 50% of the O_3 column is determined by transport from the stratosphere, and the stratospheric O_3 source dominates at higher latitudes. Simulated wind fields in the region agree well with ECMWF analyses presented by *Krishnamurti et al.* [1993]. Further, the strong vertical wind shear in SH tropical latitudes, leading to 180° different wind directions as also shown by *Thompson et al.* [1996a], is reproduced well by the model.

We have compared modeled O_3 distributions over the Atlantic Ocean with a latitudinal and vertical O_3 distribution measured in September/October 1988 [*Smit et al.*, 1990]. The measurements and calculations show a column of relatively O_3-low air near 10°N, associated with the convective ITCZ, where photochemical destruction predominates. They also show regions with much higher O_3 mixing ratios north and south of the ITCZ. Model results indicate that these are due to downward transports of O_3 from the stratosphere and to photochemical O_3 formation in the troposphere. The measured and modeled O_3 distributions agree reasonably well in the upper and middle troposphere, whereas the modeled O_3 variability is of the same order as the measured variability.

However, absolute O_3 levels over the SH tropical Atlantic Ocean appear to be generally underestimated by the model. Notably, a discrepancy is found in the lower troposphere between about 20° and 0°S, where mixing ratios measured by *Smit et al.* [1990] are up to a factor of 2 higher than the model results. Further, simulated free tropospheric O_3 mixing ratios over Ascension Island are significantly lower than measured [*Thompson et al.*, 1996a]. Note, however, that the free tropospheric O_3 levels measured on board the *Polarstern* at the same latitude are also somewhat lower, about 10–20 ppbv. Further, O_3 abundances measured during TRACE A, which are associated with South American biomass burning emissions, appear rather high compared to climatological values [*Fishman et al.*, 1996b]. Nevertheless, tropospheric O_3 columns over the SH Atlantic Ocean from the TOMS/SAGE climatology are up to 10 DU higher than calculated columns [*Fishman et al.*, 1990; *Hudson et al.*, 1995]. This discrepancy may be partly due to the tropopause height definition, which is a critical parameter in tropospheric O_3 column calculations as well as satellite data retrieval. Nevertheless, it is likely that the model underestimates photochemical production of O_3 in the area because higher hydrocarbons released by biomass burning have not been considered. First, higher hydrocarbon emissions may lead

to a more efficient in situ production of O_3 near the source regions. Model results indicate that over the source regions, in the lower troposphere, strong O_3 production occurs. Second, some of these hydrocarbons and reservoir species such as PAN have lifetimes of a few days to weeks and may lead to additional O_3 production during transport in the lower- and higher-altitude flows over the Atlantic Ocean. This is corroborated by the fact that our model simulates net O_3 destruction over the South Atlantic Ocean, whereas a net O_3 production of 1–2 DU d^{-1} has been derived from TRACE A measurements.

Acknowledgments. This research is part of the SINDICATE project, which is supported by the European Commission (DG XII), and of the joint research with the Center for Clouds, Chemistry, and Climate (C^4) at the University of California, San Diego (C^4 paper 173). We thank the Max-Planck-Institute for Meteorology in Hamburg for the use of computer facilities and support.

References

Benkovitz, C. M., M. T. Scholtz, J. Pacyna, L. Tarrason, J. Dignon, E. C. Voldner, P. A. Spiro, J. A. Logan, and T. E. Graedel, Global gridded inventories of anthropogenic emissions of sulfur and nitrogen, *J. Geophys. Res.*, *101*, 29,239–29,253, 1996.

Brost, R. A., J. Feichter, and M. Heimann, Three-dimensional simulation of ^{7}Be in a global climate model, *J. Geophys. Res.*, *96*, 22,423–22,445, 1991.

Chen, C. T., and E. Roeckner, Validation of the Earth radiation budget as simulated by the Max Planck Institute for Meteorology general circulation model ECHAM4 using satellite observations of the Earth Radiation Budget Experiment, *J. Geophys. Res.*, *101*, 4269–4287, 1996.

Connors, V. S., and H. G. Reichle, Space shuttle views changing carbon monoxide in lower atmosphere, *Eos*, *77*, 466–467, 1996.

Crutzen, P. J., Ozone in the troposphere, in *Composition, Chemistry, and Climate of the Atmosphere*, edited by H. B. Singh, pp. 349–393, Van Nostrand Reinhold, New York, 1995.

Crutzen, P. J., and M. O. Andreae, Biomass burning in the tropics: Impact on atmospheric chemistry and biogeochemical cycles, *Science*, *250*, 1669–1678, 1990.

Diab, R. D., et al., Vertical ozone distribution over southern Africa and adjacent oceans during SAFARI-92, *J. Geophys. Res.*, *101*, 23,823–23,833, 1996.

Feichter, J., R. A. Brost, and M. Heimann, Three-dimensional modeling of the concentration and deposition of ^{210}Pb aerosols, *J. Geophys. Res.*, *96*, 22,447–22,460, 1991.

Feichter, J., E. Kjellström, H. Rodhe, F. Dentener, J. Lelieveld, and G. J. Roelofs, Simulation of the tropospheric sulfur cycle in a global climate model, *Atmos. Environ.*, *30*, 1693–1707, 1996.

Fishman, J., C. E. Watson, J. C. Larsen, and J. A. Logan, Distribution of tropospheric ozone determined from satellite data, *J. Geophys. Res.*, *95*, 3599–3617, 1990.

Fishman, J., K. Fakhruzzaman, B. Cros, and D. Nganga, Identification of widespread pollution in the southern hemisphere deduced from satellite analyses, *Science*, *252*, 1693–1696, 1991.

Fishman, J., J. M. Hoell Jr., R. D. Bendura, R. J. McNeal, V. W. J. H. Kirchhof, NASA GTE TRACE A Experiment (September–October 1992): Overview, *J. Geophys. Res.*, *101*, 23,865–23,879, 1996a.

Fishman, J., V. G. Brackett, E. V. Browell, and W. B. Grant, Tropospheric ozone derived from TOMS/SBUV measurements during TRACE A, *J. Geophys. Res.*, *101*, 24,069–24,082, 1996b.

Ganzeveld, L. N., and J. Lelieveld, Dry deposition parameterization in a chemistry-general circulation model and its influence on the distribution of chemically reactive trace gases, *J. Geophys. Res.*, *100*, 20,999–21,012, 1995.

Hao, W. M., and M. H. Liu, Spatial and temporal distribution of tropical biomass burning, *Global Biogeochem. Cycles*, *8*, 495–503, 1994.

Haskins, R. D., T. P. Barnett, M. M. Tyree, and E. Roeckner, Comparison of cloud fields from atmospheric general circulation model, in situ, and satellite measurements, *J. Geophys. Res.*, *100*, 1367–1378, 1995.

Hoerling, M. P., T. K. Schaack, and A. J. Lenzen, A global analysis of stratospheric-tropospheric exchange during northern winter, *Mon. Weather Rev.*, *121*, 162–172, 1993.

Holton, J. R., P. H. Haynes, M. E. McIntyre, A. R. Douglas, R. B. Rood, and L. Pfister, Stratosphere-troposphere exchange, *Rev. Geophys.*, *33*, 403–439, 1995.

Hudson, R. D., J. H. Kim, and A. M. Thompson, On the derivation of tropospheric column ozone from radiances measured by the total ozone mapping spectrometer, *J. Geophys. Res.*, *100*, 11,137–11,145, 1995.

Intergovernmental Panel on Climate Change (IPCC), *Climate Change*, edited by J. T. Houghton, L. G. Meira Filho, J. Bruce, H. Lee, B. A. Callander, E. Haites, N. Harris, and K. Maskell, Cambridge Univ. Press, New York, 1994.

Jacob, D. J., et al., Origin of ozone and NO_x in the tropical troposphere: A photochemical analysis of aircraft observations over the South Atlantic basin, *J. Geophys. Res.*, *101*, 24,235–24,250, 1996.

Jeuken, A. B. M., P. C. Siegmund, L. C. Heijboer, J. Feichter, and L. Bengtsson, On the potential of assimilating meteorological analyses in a global climate model for the purpose of model validation, *J. Geophys. Res.*, *101*, 16,939–16,950, 1996.

Kim, J. H., R. D. Hudson, and A. M. Thompson, A new method of deriving time-averaged tropospheric column ozone over the tropics using total ozone mapping spectrometer (TOMS) radiances: Intercomparison and analysis using TRACE A data, *J. Geophys. Res.*, *101*, 24,317–24,330, 1996.

Kirchhoff, V. W. J. H., J. R. Alves, and F. R. da Silva, Observations of ozone concentrations in the Brazilian cerrado during the TRACE A field expedition, *J. Geophys. Res.*, *101*, 24,029–24,042, 1996.

Komhyr, W. D., S. J. Oltmans, P. R. Franchois, W. F. J. Evans, and W. A. Matthews, The latitudinal distribution of ozone to 35 km altitude from ECC ozonesonde observations, 1985–1987, in *Ozone in the Atmosphere*, edited by R. D. Bojkov and P. Fabian, pp. 147–150, A. Deepak, Hampton, Va., 1989.

Koppmann, R., R. Bauer, F. J. Johnen, C. Plass, and J. Rudolph, The distribution of light nonmethane hydrocarbons over the Mid-Atlantic: Results of the Polarstern Cruise ANT VII/1, *J. Atmos. Chem.*, *15*, 215–234, 1992.

Krishnamurti, T. N., H. E. Fuelberg, M. C. Sinha, D. Oosterhof, E. L. Bensman, and V. B. Kumar, The meteorological environment of the tropospheric ozone maximum over the tropical South Atlantic Ocean, *J. Geophys. Res.*, *98*, 10,621–10,641, 1993.

Krishnamurti, T. N., M. C. Sinha, M. Kanamitsu, D. Oosterhof, H. Fuelberg, R. Chatfield, D. J. Jacob, and J. Logan, Passive tracer transport relevant to the TRACE A experiment, *J. Geophys. Res.*, *101*, 23,889–23,907, 1996.

Lelieveld, J., and P. J. Crutzen, Influences of cloud photochemical processes on tropospheric ozone, *Nature*, *343*, 227–233, 1990.

Lelieveld, J., and R. van Dorland, Ozone chemistry changes in the troposphere and consequent radiative forcing of climate, in *Atmospheric Ozone as a Climate Gas*, edited by W. C. Wang and I. S. A. Isaksen, pp. 227–258, Springer-Verlag, New York, 1995.

Levy, H., II, W. J. Moxim, and P. S. Kasibhatla, A global three-dimensional time dependent lightning source of NO_x, *J. Geophys. Res.*, *101*, 22,911–22,922, 1996.

Lindesay, J. A., M. O. Andreae, J. G. Goldammer, G. Harris, H. J. Annegarn, M. Garstang, R. J. Scholes, and B. W. van Wilgen, International Geosphere-Biosphere Programme/International Global Atmospheric Chemistry SAFARI-92 field experiment: Background and overview, *J. Geophys. Res.*, *101*, 23,521–23,530, 1996.

Logan, J. A., Trends in the vertical distribution of ozone: An analysis of ozonesonde data, *J. Geophys. Res.*, *99*, 25,553–25,585, 1994.

Logan, J. A., and V. W. J. H. Kirchhoff, Seasonal variations of tropospheric ozone at Natal, Brazil, *J. Geophys. Res.*, *91*, 7875–7882, 1986.

Lowe, D. C., C. A. Brenninkmeijer, G. W. Brailsford, K. R. Lassey, A. J. Gomez, and E. G. Nisbet, Concentration and ^{13}C records of atmospheric methane in New Zealand and Antarctica: Evidence for changes in methane sources, *J. Geophys. Res.*, *99*, 16,913–16,925, 1994.

Oltmans, S. J., and H. Levy II, Surface ozone measurements from a global network, *Atmos. Environ.*, *28*, 9–24, 1994.

Papenbrock, T., F. Stuhl, K. P. Müller, and J. Rudolph, Measurement of gaseous HNO_3 over the Atlantic Ocean, *J. Atmos. Chem.*, *15*, 369–379, 1992.

Pickering, K. E., et al., Convective transport of biomass burning emissions over Brazil during Trace A, *J. Geophys. Res.*, *101*, 23,993–24,012, 1996.

Price, C., and D. Rind, A simple lightning parameterization for calculating global lightning distributions, *J. Geophys. Res.*, *97*, 9919–9933, 1992.

Rasch, P. J., and D. Williamson, Computational aspects of moisture transport in global models of the atmosphere, *Q. J. R. Meteorol. Soc.*, *116*, 1071–1090, 1990.

Roeckner, E., T. Siebert, and J. Feichter, Climatic response to anthropogenic sulfate forcing simulated with a general circulation model, in *Aerosol Forcing of Climate*, edited by R. J. Charlson and J. Heintzenberg, pp. 349–362, John Wiley, New York, 1995.

Roeckner, E., K. Arpe, L. Bengtsson, M. Christoph, M. Claussen, L. Dümenil, M. Esch, M. Giorgetta, U. Schlese, and U. Schulzweida, The atmospheric general circulation model ECHAM-4: Model description and simulation of present-day climate, *Rep. 218*, Max-Planck-Inst. for Meteorol., Hamburg, Germany, 1996.

Roelofs, G. J., and J. Lelieveld, Distribution and budget of O_3 in the troposphere calculated with a chemistry-general circulation model, *J. Geophys. Res.*, *100*, 20,983–20,998, 1995.

Roelofs, G. J., and J. Lelieveld, Model study of the influence of cross-tropopause O_3 transports on tropospheric O_3 levels, *Tellus*, *Ser. B*, *49*, 38–55, 1997.

Smit, H. G. J., D. Kley, S. McKeen, A. Volz, and S. Gilge, The latitudinal and vertical distribution of tropospheric ozone over the Atlantic Ocean in the southern and northern hemispheres, in *Ozone in the Atmosphere*, edited by R. D. Bojkov and P. Fabian, pp. 419–422, A. Deepak, Hampton, Va., 1989.

Smit, H. G. J., S. Gilge, and D. Kley, The meridional distribution of ozone and water vapor over the Atlantic Ocean between 30°S and 52°N in September/October 1988, in *Physico-Chemical Behaviour of Atmospheric Pollutants*, edited by G. Restelli and G. Angeletti, pp. 630–637, Kluwer Acad., Norwell, Mass., 1990.

Smit, H. G. J., S. Gilge, and D. Kley, Ozone profiles over the Atlantic Ocean between 36°S and 52°N in March/April 1987 and September/October 1988, *Jül Ber. 2567*, Forsch. Jülich, West Germany, 1991.

Smit, H. G. J., W. Straeter, and D. Kley, The evaluation of ECC-sondes under quasi flight conditions in the environmental simulation chamber at Juelich, paper presented at EUROTRAC Symposium 94, EUROTRAC, Garmisch-Partenkirchen, Bavaria, Germany, 1994.

Talbot, R. W., et al., Chemical characteristics of continental outflow over the tropical South Atlantic Ocean from Brasil and Africa, *J. Geophys. Res.*, *101*, 24,187–24,202, 1996.

Thompson, A. M., K. E. Pickering, D. P. McNamara, M. R. Schoeberl, R. D. Hudson, J. H. Kim, E. V. Browell, J. Fishman, V. W. J. H. Kirchhoff, and D. Nganga, Where did tropospheric ozone over southern Africa and the tropical Atlantic come from in October 1992? Insights from TOMS, GTE/TRACE-A, and SAFARI-92, *J. Geophys. Res.*, *101*, 24,251–24,278, 1996a.

Thompson, A. M., et al., Ozone over southern Africa during SAFARI-92/TRACE A, *J. Geophys. Res.*, *101*, 23,793–23,807, 1996b.

Tiedtke, M., A comprehensive mass flux scheme for cumulus parameterization in large-scale models, *Mon. Weather Rev.*, *117*, 1779–1800, 1989.

Weller, R., R. Lilisschkis, O. Schrems, R. Neuber, and S. Wessel, Vertical ozone distribution in the marine atmosphere over the central Atlantic Ocean (56°S–50°N), *J. Geophys. Res.*, *101*, 1387–1399, 1996.

Winkler, P., Surface ozone over the Atlantic Ocean, *J. Atmos. Chem.*, *7*, 73–91, 1988.

World Meteorological Organization (WMO), Scientific assessment of depletion: 1994, Global ozone research and monitoring project, *Rep. 37*, Geneva, Switzerland, 1995.

Yienger, J. J., and H. Levy II, Empirical model of global soil-biogenic NO_x emissions, *J. Geophys. Res.*, *100*, 11,447–11,464, 1995.

D. Kley and H. G. J. Smit, Institute for Chemistry of the Polluted Atmosphere (ICG-2), P.O. Box 1913, D-52425 Jülich, Germany. (e-mail: d.kley@kfa-uelich.de; h.smit@kfa-juelich.de)

J. Lelieveld and G.-J. Roelofs, Institute for Marine and Atmospheric Research Utrecht (IMAU), Princetonplein 5, 3584 CC Utrecht, The Netherlands. (e-mail: lelieveld@fys.ruu.nl; roelofs@fys.ruu.nl)

(Received September 27, 1996; revised February 4, 1997; accepted February 4, 1997.)